

## Dense ceramic membranes: A review of the state of the art

V. KOZHUKHAROV, M. MACHKOVA, N. BRASHKOVA

University of Chemical Technology and Metallurgy- Sofia Sofia - 1756, Bulgaria

During the past several years the concepts of oxygen permeation through mixed valency ceramic membranes possess special interest. In this context, a classification and brief review of the major membrane ceramic materials will be presented. The focus will be on dense ceramic membranes as elements for advanced application. A discussion will be proposed for mixed conductor ceramics as perovskite  $ABO_3$  compounds. Dense membranes on perovskite base are the object of the present review and some details about processing and characterization of double (A- and B-site) substituted  $La_{1-x}Sr(Ba)_xCo_{0.8}Fe_{0.2}O_{3-d}$  perovskites will be presented.

*Key words: dense ceramic membranes, perovskites, oxygen transport, processing, characterization*

### Membranas cerámicas densas: Una revisión del estado de la técnica

El concepto de permeación de oxígeno a través de membranas cerámicas de valencia mixta, ha venido adquiriendo especial relevancia a lo largo de los últimos años. En este contexto se hace se efectúa una clasificación y breve revisión de los materiales cerámicos más relevantes utilizados como membranas. En particular se orienta la descripción hacia las membranas cerámicas densas para aplicaciones avanzadas. Se propone un análisis de los conductores cerámicos mixtos, como los compuestos de tipo perovskita  $ABO_3$ . Se realiza una revisión de los materiales de este tipo existentes, así como se describen algunos aspectos sobre el procesamiento y caracterización de las perovskitas tipo  $La_{1-x}Sr(Ba)_xCo_{0.8}Fe_{0.2}O_{3-d}$  doblemente sustituidas (lugares A- y B-)

*Palabras clave: emembranas cerámicas densas, perovskitas, transporte de oxígeno, procesamiento, caracterización*

### 1. INTRODUCTION

In a chemical reactor the fluid media can be effectively separated using both porous and dense inorganic membranes. The porous ceramic membranes are very attractive for gas separation industry and techniques [1,2].

New developments on dense ceramic membranes are very actual at present. Dense membranes are suitable for application of atomic, ionic, mixed (electron and ion) or molecular diffusion. They possess high selectivity but the permeability is relatively low. Ion permeability level can be improved by decreasing the membrane thickness and increasing the functional temperature. Possible applications in the field of chemical technology roughly can be indicate as follows:

- for oxygen separation and production of oxygen from air;
- for partial oxidation of light hydrocarbons in the field of chemical processing;
- for syngas ( $CO$  and  $H_2$ ) production;
- for waste reduction and environmental technology application;
- for high temperature electrocatalysis on base of NEMCA effect (i.e. electrochemical oxygen pump).

The present review is an attempt to follow the state of processing and development of dense ceramic membranes as well as to classify them; to focus the attention on new concepts for research and development of dense ceramic membranes from the perovskite family and to present actual experimental data in the author's laboratory on the problem discussed.

### 2. MEMBRANES CLASSIFICATION

The IUPAC's nomenclature for porous materials [3] is well known. The classification is well accepted in the world scientific society. In dependence of the pore diameter the membranes are classified as macroporous, mesoporous, microporous and dense [4,5]. A short description of membrane classification on the base of porosity level is presented in ref. [2]; for commercialized inorganic membranes the problem is discussed in ref.[1]. An attempt to outline view and useful classification of porous and dense ceramic membranes is presented in ref. [2, 4].

### 3. DENSE MEMBRANES

According to Burggraaf et al. [6] the dense membranes can be distinguished into three groups:

- ceramic (solid electrolyte type);
- metal and alloys and
- liquid immobilized (LIM) membranes, respectively.

As is marked above the accent of the present work is within solid electrolyte type ceramic membranes. There is no attempt to discuss dense metal and LIM membranes since they are outside the scope of the present work. It only mentioned that the membranes on metal base are generally studied for hydrogen separation and electrocatalysis; the second one are predominantly dual phase composite membranes achieved after impregnation with molten salt mixtures.

Dense ceramic membranes can be divided into two kinds depending on the nature and behaviour of the matter. There are namely :

- solid oxide electrolytes and
- the mixed ionic- electronic conductors, respectively.

### 3.1. Dense membranes on solid oxide electrolyte base

Solid electrolytes usually are classified according to the ion species and conductivity nature. According to Vayenas et al. [7] the most important ion conductors are:

- $O_2^-$  &  $O^-$  ion conductors, e.g. extended family of solid solutions of metal oxides (II or III valency state) incorporated into metal oxides (IV valency state) e.g. YSZ ceramics. The cubic  $\delta$ -phase of  $Bi_2O_3$  is the best oxygen ion conductor known.
- $H^+$  conductors, e.g.  $H^+$ - substituted  $\beta''$ -  $Al_2O_3$  or  $SrCeO_3$ -based compounds;
- $Na^+$  conductors, e.g. non- stoichiometric  $\beta''$ -  $Al_2O_3$  compounds after substitution of Na ions; high conductivity in the temperature range from 150-C to 300-C ;
- $Ag^+$  conductors, e.g. as a-  $AgI$  and  $RbAg_4I_5$  compounds; working range from 150-C to 350-C.
- $F^-$  conductors, e.g.  $PbF_2$  well known from Faraday's experiments since 1834.

Solid electrolyte membranes can operate in two different modes :

- as solid oxide fuel cell (SOFC) and
- as electrochemical oxygen pump.

It is well known that the primary purpose of a SOFC operation is the electrical energy generation. In this context there are a lot of experiments and concepts published. State-of- the art, technological problems and future lines of research of SOFC in Europe is discussed by Zegers [8]. As a correlation the status of SOFC development in USA [9], Japan [10] and Australia [11] is presented, as well.

It is necessary to mention that opposite of Molten Carbonate Fuel Cell (MCFC), SOFC has not any problem with the electrolyte operation. The solid cell work as the cathode is exposed to air. Driving force for oxygen transport is the oxygen pressure gradient across the membrane, as shown in figure 1a. Undoubtedly, some chemicals can be co- generated parallel with electricity. The process can be accomplished if a proper choice of reagents for the oxidation reaction on the anode interface boundary is performed.

Figure 1b shows a dense oxide membrane reactor (solid state oxygen pumping and a removal system) for partial oxidation. The process is possible when oxygen is transported from one side of the ceramic membrane to the other side. As Figure 1b illustrates this is accomplished when a potential less than one volt is applied across the membrane at about 800 - 900-C. Schematically, the device work described as follows. Two oxygen ions are removed from the solid oxide electrolyte at the anode/electrolyte interface and are oxidized into an oxygen molecule. At the same time, an oxygen molecule is reduced to two oxygen ions at the cathode/ electrolyte interface. These oxygen ions migrate to the anode/electrolyte interface via oxygen ion vacancies (Wagner theory). The net result of the process is an oxygen transport through the dense membrane. The transport is accomplished after the application of electric potential at high temperature only. When air is present at the cathode, the system will act as an oxygen generator.

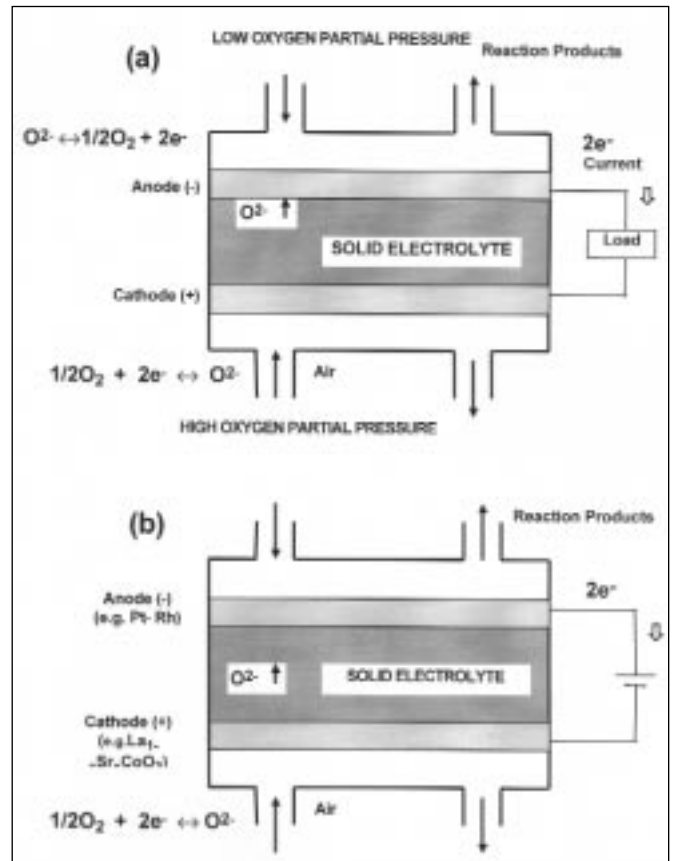


Figure 1. Operating principle of (a)- solid oxide fuel cell (SOFC) and (b) electrochemical oxygen pump (OP).

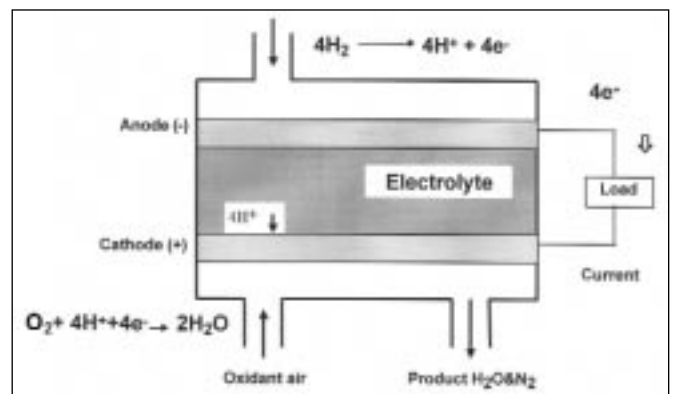


Figure 2. Schematic cross section of a single hydrogen- oxygen fuel cell, the major component of a fuel cell stack.

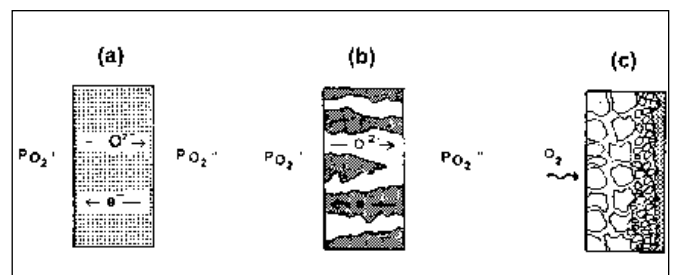


Figure 3. Types of mixed (ionic- electronic) conducting dense ceramic membranes a) single phase membrane, b) dual- phase (cermet) membrane and c) asymmetric (porous graded support and dense barrier layer on top) hybrid membranes; reproduced from ref.[12].

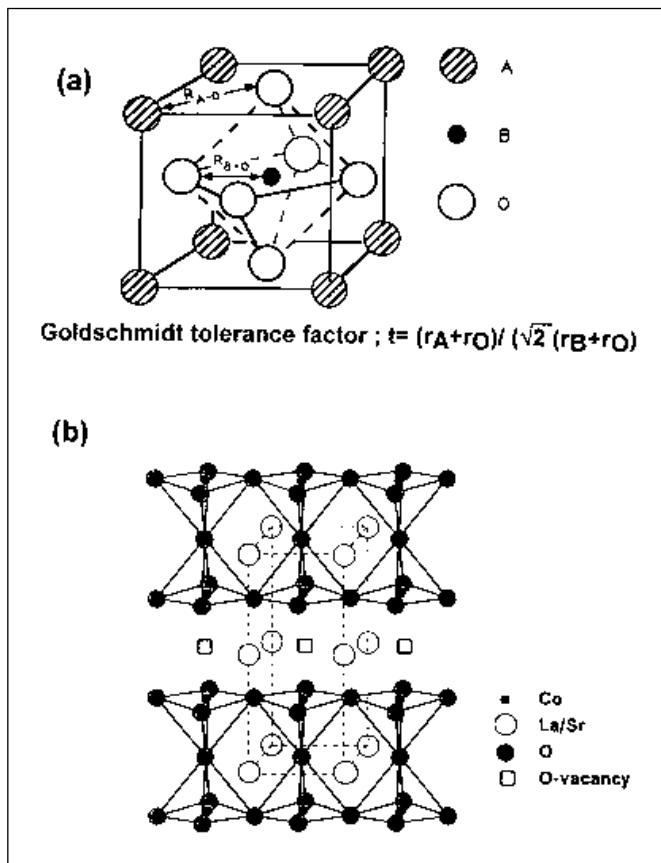


Figure 4. Ideal perovskite structures for (a) -  $ABO_3$  unit and for (b)-  $(La_{1-x}Sr_xCoO_{3-\delta})$  ( $x=0.5$  and  $x=0.7$ ) ; (b) part is a reproduction according to van Doorn et al.[12, 22]

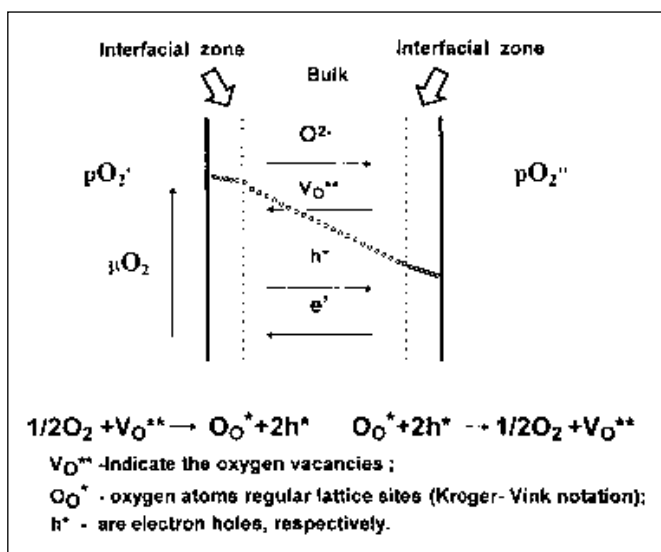


Figure 5. Representation of relevant fluxes through a ceramic membrane upon applying a different oxygen partial pressure ( $pO_2' > pO_2''$ ). Schematic representation of the gradient in the oxygen chemical potential ( $\mu_{O_2}$ ), at various zones during steady state oxygen permeation. After adaptation from Bouwmeester et al. [27].

Undoubtedly, the methane conversion to higher hydrocarbons and/or syngas ( $CO, H_2$ ) reaction product outlet, are subject of scientific and industrial interest.

It is also possible to generate electrical energy if we have  $H^+$ -exchange membrane (PEM). Figure 2 shows a single hydrogen/oxygen fuel cell on proton exchange phenomenon. Two molecules of  $H_2$  are combined with each molecule of  $O_2$  to produce two molecules of water. In addition electrical energy is produced as is shown in the figure.

As we cited above, the electrons nonconductivity nature e.g. of zirconia makes unsuitable for commercial separation of oxygen. The architectures shown in figure 1 possess electrodes with an external short circuit that makes the system impractical.

### 3.2. Mixed ionic- electronic conductors as dense membranes

An alternative of the solid electrolytes discussed above are the perovskite ceramic membranes. These materials are mixed ionic and electronic conductors. Except high level of ionic conductivity the perovskites exhibit a significant electronic conductivity ( $\sigma_{ion} < \sigma_{el}$ ). Namely, the electronic conductivity of the matter stimulates an internal short-circuit behaviour of the system. As a result these mixed (ion- electron) conducting membranes do not need electrodes and an external circuit as was shown in the case for solid electrolytes in figures 1 and 2. Because of the oxygen partial pressure gradient, then the oxygen anions will permeate from the high to the lower partial pressure side of the membrane surface. Opposite of the oxygen anions migration a flux of electrons and/or electron holes is executed too. This is well illustrated in figure 3 where different membrane concepts for oxygen ion transport is presented after Bouwmeester and Burggraaf [12].

The ceramic membranes are well known in electrochemical applications. As we discussed above the mobile species are both types of ions: cations (e.g.  $Li^+, Ag^+$  etc.) and anions (e.g.  $O^{2-}$ ). The flux of ions is driven either by applied electric field (NEMCA effect [7,13-15]) or by a gas pressure gradient. The materials with virtually high permselectivity at high temperature treatment to oxygen are YSZ [7, 15] and some perovskites [16-19] as well.

A high mixed conductivity was established, both ionic and electronic of ceramic samples, after the pioneering work of Teraoka et. al. [20]. A perovskite- type oxide  $LaCo(Fe)O_3$  was doped with Sr(II) ions on La(III)- site. As a result solid solutions of  $La_{1-x}Sr_xCo_{1-y}Fe_yO_{3-\delta}$  (where  $x=y=0-1$ ) are generated. Since  $\delta$  denotes the average number of vacant oxygen sites per unit cell this is an indicator of the level of non- stoichiometry [21]. A- site heterovalency substitution in the perovskite structure will stimulate the creation of oxygen vacancies and an increasing of electron holes (p-type doping effect) will be achieved.

#### 3.2.1. PEROVSKITE STRUCTURE AND OXYGEN TRANSPORT

To understand better the mechanism of oxygen transport, we need to consider in short the perovskite crystal structure. The ideal perovskite structure  $ABO_3$  is presented in figure 4a. This is a typical cubic structure with  $BO_6$  octahedral incorporation in it. By B is marked a 3d- transition element and A is either a lanthanide or an alkaline-earth metal cation. Evidently the A cations occupy the corner site and B cations occupy the center of the unit cell. Oxygen ions around the B cation are

found on the faces of the unit cell and an oxygen sublattice is built. For oxygen inner transport a number of oxygen empty space into the oxygen sublattice is required. These empty spaces are typical oxygen vacancies as is shown in figure 4b according to ref. [22]. In other words they are affected as bulk oxygen carries across the body. According to Russek [23] there are two principal means in creation of oxygen vacancies in ceramic materials, namely:

- site substitution and
- interaction with the gas phase.

In the case of site structural substitution the value of Goldschmidt factor ( $t = (r_A + r_O) / (\sqrt{2}(r_B + r_O))$ ) is the important one. This factor for a cubic perovskite structure is close to 1. Stable perovskite structure require  $t$  value in the range from 0.75 to 1. In the case of large lattice distortion other crystal symmetries (hexagonal, orthorhombic or rhombohedral [24, 25]) will be developed. A substitution of host cation at A-site with cations of lower formal valence will stimulate increasing of oxygen vacancies. As a result, a creation of defects with positive electric charge will appear in the body. Once created the oxygen vacancies are free to move among energetically equivalent crystallographic sites. Oxygen transport in the perovskites is accepted to occur via a vacancy transport mechanism [26,12].

If we assume that oxygen vacancies are the mobile ionic defects then the oxygen ion conductivity can be given by the Nernst- Einstein equation:

$$\sigma_{\text{ion}} = \frac{4F^2 C_v D_v}{RT}, \quad (1)$$

where  $F$  is the Faraday constant,  $C_v = \delta/V_m$  is the oxygen ions vacancy concentration ( $\delta = [V_{\text{O}}]$ ;  $V_m$  is the perovskite molar volume) and  $D_v$  is the vacancy diffusivity. If we rejected the total electronic conductivity ( $\sigma_e + \sigma_h$ ), then the oxygen flux can be calculated by Wagner [26] equation:

$$j_{\text{O}_2} = \frac{1}{16 F^2 L} \frac{\ln p'_{\text{O}_2}}{\ln p''_{\text{O}_2}} \int \sigma_{\text{O}_2} d \ln p_{\text{O}_2}. \quad (2)$$

At the membrane surface the reaction of oxygen incorporation will take place as is shown in figure 5. There are well illustrated zones that belong to the central bulk zone (Wagner) and to the adjacent interfacial zones. These zones schematically represent both the solid state bulk diffusion and the surface oxygen exchange of the membrane. These contributions are in close relation to the oxygen flux level. The driving force is the oxygen chemical potential ( $\Delta\mu_{\text{O}_2}$ ) that can be expressed, as:

$$\mu_{\text{O}_2} = \mu^{\circ}_{\text{O}_2} + RT \ln p_{\text{O}_2}, \quad (3)$$

where  $\mu^{\circ}_{\text{O}_2}$  is a reference value of chemical potential at temperature  $T$ . Solid state diffusion determines the rate of oxygen transfer crosswise the membrane. Upon reducing thickness the flux is controlled by a limited transfer of oxygen across the interfaces [12, 27].

To maximize flux all oxygen vacancies have to participate at a higher level of the carrier mobility. In this context, a cubic perovskite structure will maximize the number of vacancies available for oxygen transport. However, important parameters are the temperature and the effective oxygen partial pressure gradient applied.

The creation of oxygen vacancies by interaction with the gas phase is also possible by 3d-transition metal containing perovskites with a general formula  $\text{LaBO}_3$  ( $B = \text{V, Cr, Fe, Co, Ni}$ ) [28]. These trends follow reducibility of the related binary transition metal oxides [23, 29].

Another details concerning oxygen permeation modelling of perovskites are discussed in ref. [30] on the base of the point defect model, in ref. [27] on the base of Wagner's theory and surface exchange kinetics and in ref. [12] on the base of vacancy ordering and the  $p_{\text{O}_2}$  gradient behaviour.

### 3.2.2. MEMBRANE PARAMETERS AND REACTOR DESIGN

Ceramic membranes on perovskite base can be prepared, if we follow the calcination procedure of the obtained high disperse black powder. Detailed technological steps are presented in ref. [21, 31]. Generally, the dense ceramic membranes can be shaped into two architectures:

- planar geometry as ceramic disk or slab form and
- tubular support type.

Figure 6 shows permeation reactors using disk membrane structure with disk thickness of about 1.0 mm. According to ten Elshof [21] this is a quartz reactor in which a 1.0 mm thick quartz glass ring is used to seal the membrane at 1310- 1330K. A pretreatment procedure is recommended, using a CO- containing atmosphere. Gas helium is supplied to the permeates side of the membrane sample as is shown in figure 6a. The oxygen partial pressure can be varied by adjusting the total flow rate, e.g. at the feed side it could vary between 0.01 and 1.0 bar by mixing of air,  $\text{N}_2$  and  $\text{O}_2$ .

Another electrochemical reactor which facilitates the transfer of oxygen is proposed according to ref. [32]. The reactor design is very close to the permeation reactor, shown in figure 6b and described in ref. [21, 33]. In this experimental unit the oxygen is driven across the membrane from an oxygen containing gas to an oxygen consuming gas e.g. methane as a reactant gas. Composition analysis of the permeate gas stream can be performed by gaschromatograph (GC) as is arranged in the figure 7. The oxygen partial pressure of both retarded and permeate streams is continuously measured by YSZ- based oxygen sensors [21, 34]. The oxygen fluxes can be calculated according to the mass balance. Precise data for theory and experiment are presented in ref. [21] regarding the oxygen transport through membranes for permeation at air/helium gradients and air/CO,  $\text{CO}_2$  gradients, as well.

As figure 8 shows, ceramic membranes can be shaped and into a hollow- tube reactor. According to Balachandran et al. [35] in this type of reactor the air flows on the outside of the membrane and methane flows through on the inside. The membrane is permeable to oxygen at high temperatures and it reacts with the methane inside of the reactor surface. Another details about tubular shaped membrane reactor in double-pipe configuration and membrane reactor design consideration and challenges are surveyed in ref. [6] and in ref. [36], respectively. Honeycomb, corrugated or cellular [37] configurations of reactors are also possible. Using greater surface areas for reaction carried out is an advantage in the new chemical processes of oxidation based on membrane reactors discussed.

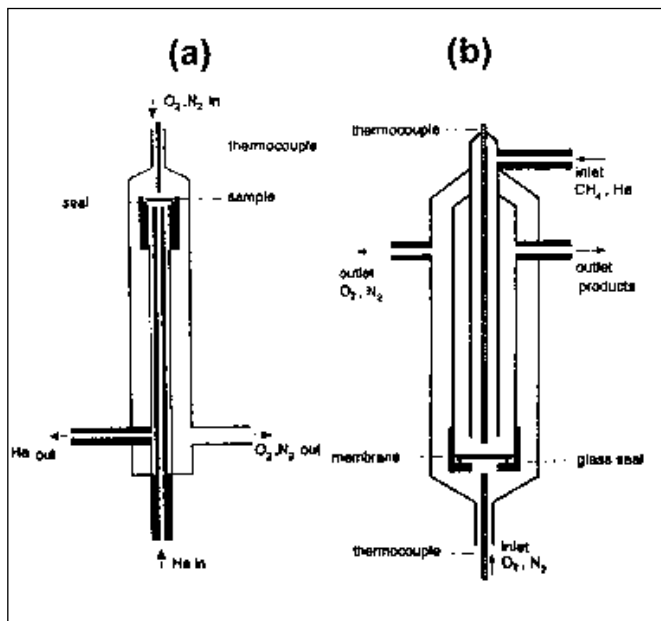


Figure 6. The permeation reactor unit (a)- Permeation in air/helium gradients and (b)- Permeation in a catalytic reactor exposed by methane (He) atmosphere; according to ten Elshof [21].

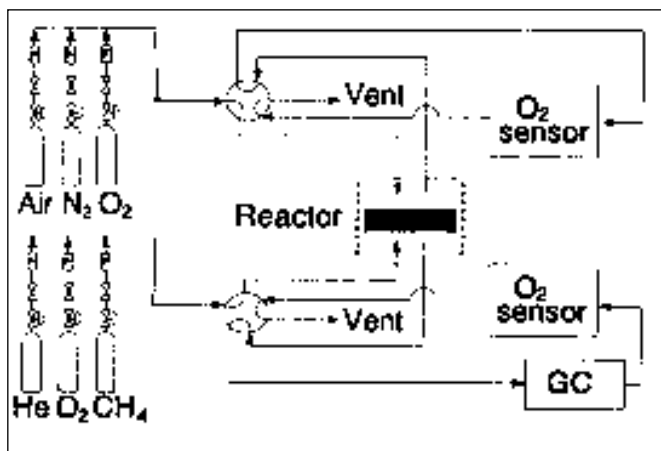


Figure 7. Schematic diagram of the experimental set up; reproduced from ref. [21].

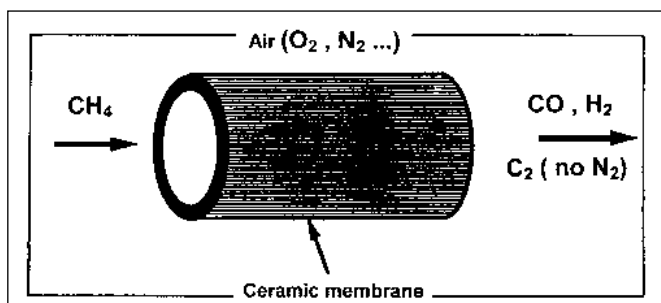


Figure 8. Hollow-tube reactor; reproduced from Balachandran et al. [35].

#### 4. PROCESSING AND CHARACTERIZATION OF PEROVSKITE MEMBRANES

Detailed research about mixed conducting lanthanum containing ceramic compositions with general formula  $\text{La}_{1-x}\text{Sr}(\text{Ba})_x\text{Co}_{0.8}\text{Fe}_{0.2}\text{O}_{3-\delta}$  is described elsewhere [31]. Here we would like only to discussed in short the processing track and the characterization procedures of double substituted perovskite membranes.

##### 4.1. Powder processing and membrane preparation track

In our experiments samples with formula  $\text{La}_{1-x}\text{Sr}(\text{Ba})_x\text{Co}_{0.8}\text{Fe}_{0.2}\text{O}_{3-\delta}$  have been prepared, where x values are 0.6, 0.4 and 0.2 respectively [31]. Figure 9 shows the procedure for ceramic powder processing and heat treatment. The starting materials used are  $\text{Sr}(\text{NO}_3)_2$ ,  $\text{Ba}(\text{NO}_3)_2$ ,  $\text{Co}(\text{NO}_3)_2 \cdot 6\text{H}_2\text{O}$ ,  $\text{Fe}(\text{NO}_3)_3 \cdot 9\text{H}_2\text{O}$  (Merck) of AnalaR grade. High disperse and homogeneous powders have been prepared using  $\text{NH}_4\text{-EDTA}$  solution; 1.5 mole per mole of metal in the solution to the clear nitrate solutions at pH values from 8 to 8.5 containing stoichiometric amounts of the reagents. As is shown in figure 9 there is a distinguished heat treatment (pyrolysis at 280-C for 2 h) of the solution decanted into quartz dishes. The so obtained high disperse black powder is referred as a complex uncalcined product.

The black mass obtained next has been head treated. It was carried out in an program electric furnace (Naber, Germany) at 925-C/ 12 h using Pt dishes covered by quartz ones. As a following step the calcined powder was ball milled using polyethylene mortar and agate balls.

After the calcination procedure the black ceramic powder has been uniaxially pressed; an isostatical pressing process at 2000 bar to obtain compact green preform samples. Finally the so press- formed bodies have been sintered at 1225-C/ 24h in an oxygen isothermal atmosphere using heating and cooling rates of 3-C / min.

The final ceramic rod has been cut, ground and polished (with 1000 Mesh SiC powder) according to a standard method. For next measurements, disks with parallel surfaces of thickness from about 1.5 mm and in 10 mm diameter have been prepared. The dense disks obtained have been ultrasonically cleaned in acetone and dried on a hot plate.

##### 4.2. Thermal characterization

Precise studies on thermal decomposition of ceramic powders have been carried. Figure 10 shows DTA, TA, TG and DTG curves for a composition and undoubtedly illustrates that the thermal decomposition runs sufficient and complete at relatively lower temperatures. The thermal reaction curves can be grouped into three regions following the curves behaviour.

The first one is from room temperature up to 260- 270-C. A well- expressed endothermic effect at  $160 \pm 10\text{-C}$  is registered. This is a contribution of the dehydration process. The weight loss checked is about 25 mg that is 8. 97% of the sample weight.

In the second region up to 670-C there are a set of endothermic peaks at DTA curves. After a correlation procedure regarding the curves behaviour it was established that the peaks are flexible in relation of their position and in depth. Namely, in

this region during the heating process both TG and DTG curves indicate a very sharp weight loss. The endothermic peaks at  $420 \pm 10$ -C and  $500 \pm 20$ -C corresponds to the decomposition of nitrate ions. The peak at 705- 710-C arises from deoxidizing and phase transition to form stable Sr/Ba- and Fe- doped lanthanum cobalt compounds. The other endothermic effects can be attributed to the processes of degradation of the organic groups introduced mainly by EDTA and simultaneously crystallization rearrangement process. Evidently the last process is highly effective above 550 up to 720-C .

Stabilization of perovskite related phases can be attributed in the third temperature region above 670-C. As a result a plateau behaviour on the curves is registered. This indicates that the solid state reactions are complete. It is well illustrated above 700-C on the TG curves, (Figure 10 - TG curve).

#### 4.3. Chemical analysis and composition control

Methods (EDX- including elements distribution, ESCA-XPS, ICP-AES and X-ray fluorescence) applied for chemical analysis and composition control show that the membrane composition after sintering are close to the nominal one. After a correlation procedure good coincidence have been established for data checked by EDX, ESCA-XPS (semiquantitative) and ICP-AES and X- ray fluorescence (quantitative) analysis.

#### 4.4. Phase characterization

The phase identification has been performed by IR spectroscopy, XRD, ND and Moessbauer spectroscopy. The data selected from JCPDS [38] show that except cubic phase other phases as distorted perovskite pseudo-cubic, hexagonal for  $\text{LaCoO}_3$  and orthorhombic for  $\text{LaFeO}_3$  are well known, too. A high degree of oxygen nonstoichiometry is inspired after A- and B-site hetero- and homo- valency substitution in the  $\text{La}_{1-x}\text{Sr}_x(\text{Ba})_x\text{Co}_{0.8}\text{Fe}_{0.2}\text{O}_{3-\delta}$  perovskites studied. The anions in such a rich in oxygen subnetwork are likely to move via an oxygen vacancy transport mechanism [26,39-41]. As we discussed above the oxygen nonstoichiometry will stimulate a more distorted perovskite- like crystal structure.

The XRD data for composition  $\text{La}_{0.6}\text{Sr}_{0.4}\text{Co}_{0.8}\text{Fe}_{0.2}\text{O}_{3-\delta}$  identify patterns values of  $\text{La}_{0.5}\text{Sr}_{0.5}\text{CoO}_{3-\delta}$  tetragonal phase [42]. Nevertheless, the cubic and the metastable perovskite-related phases are also detected. The XRD results indicate a distortion of the lattice. This effect could be treated as a function of non stable oxygen occupancy arisen after Sr(Ba)- and Fe- doping of the structure. Phase analysis shows a phase distribution almost identical to  $\text{La}_{0.6}\text{Sr}_{0.4}\text{CoO}_{3-\delta}$  [36-1393] and  $\text{La}_2\text{CoO}_4$  [34-1081] phases. Obviously, in this non- equilibrium system few perovskite- like phases will co- exist. Since the ideal cubic symmetry of the perovskite unit cell is very rare in nature the most members from the perovskite family posses deformation in different scale [24]; those stimulate the formation of low symmetry of the lattice.

The powder XRD identification of  $\text{La}_{0.6}\text{Sr}_{0.4}\text{Co}_{0.8}\text{Fe}_{0.2}\text{O}_{3-\delta}$  sample after high temperature sintering process shows presence of phases identical with those marked in [42]. Namely, co- exist phases as  $\text{La}_{0.5}\text{Sr}_{0.5}\text{CoO}_{3-\delta}$  tetragonal, cubic and metastable perovskite- related as well. The XRD data indicate that except perovskite cubic phase there is a tetragonal one with oxygen vacancies at  $d=0.25$  [42]. The observed phases (including the metastable tetragonal one) are most likely to be related to ordering of oxygen vacancies in the perovskite basic building units.

The aim of neutron scattering study was to apply the method of Rietveld profile analysis for determination of exact atomic positions in the perovskite unit cell. The experimental ND data on perovskites are published in [43-45]. The best fit of the experimental data for composition  $\text{La}_{0.6}\text{Sr}_{0.4}\text{CoO}_{3-\delta}$  was obtained for a rhombohedral unit cell (space group  $R\bar{3}c$ ,  $Z=2$ ,  $a=5.44\text{\AA}$ ,  $\alpha=60.25^\circ$  and  $x=0.30$ ) [43]. The crystal and magnetic structure of substituted lanthanum cobaltites was investigated. Each sample ( $\text{La}_{0.6}\text{Ba}_{0.4}\text{Co}_{0.9}\text{Fe}_{0.1}\text{O}_{3-\delta}$ ,  $\text{La}_{0.6}\text{Sr}_{0.4}\text{Co}_{0.9}\text{Fe}_{0.1}\text{O}_{3-\delta}$  and  $\text{La}_{0.6}\text{Ba}_{0.4}\text{CoO}_3$ ) was measured at temperatures 2, 250 and 900 K. They prove to be rhombohedral at room temperature and undergo phase transition to cubic structure at temperatures around 600K . Detailed data and a proper interpretation regarding both crystal and magnetic structures are presented in ref. [45]

As a conclusion XPS, IR and ND studies confirmed that phase close to ideal cubic one is not detected at room temperature after A- & B-site substitution. It is acceptable that the loss of oxygen will stimulate tetragonal and rhombohedral

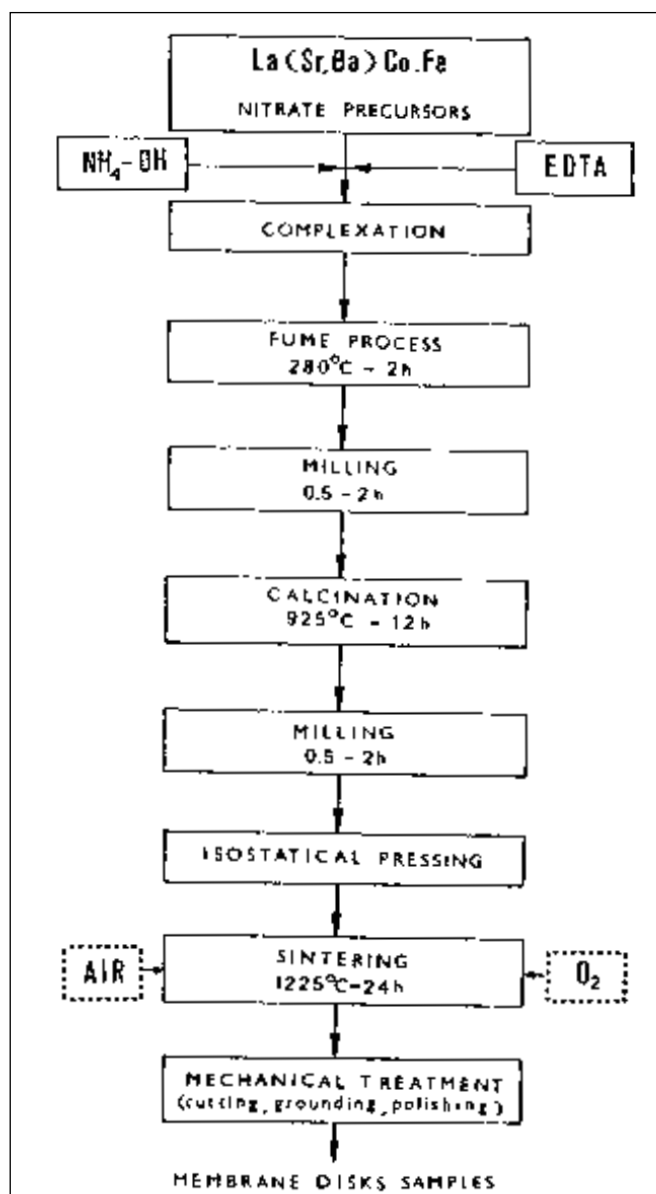


Figure 9. Flow chart of preparation of mixed-conducting oxide perovskite membranes using EDTA- modifier nitrate precursor method.

transformation of basic building units. That is a typical for solid solutions of alkali- earth metal doped cobalt- lanthanide possessing oxygen vacancies. XRD and IR experiments partly confirmed ND data. The last are more precise and covered extended temperature region of investigation. The phase analysis indicates that A- and B-site substitution stimulate deviation from the ideal perovskite structure and solid solution could be generated at low amount of lanthanum oxide.

#### 4.5. Structural characterization

##### 4.5.1. BULK STRUCTURAL CHARACTERIZATION

The applied methods (Laser Raman microprobe analysis, Moessbauer spectroscopy, Positron annihilation) serve us a useful information about membrane structure.

It was established by Raman microprobe analysis, for mem-

brane with composition  $La_{0.8}Sr_{0.2}Co_{0.8}Fe_{0.2}O_{3-\delta}$ , that there are two well- defined crystal lattices attributed to both cubic and layered tetragonal crystal phases. The obtained Raman frequency at  $456\text{ cm}^{-1}$  -  $457\text{ cm}^{-1}$  is due to the oxygen A1 mode in phase vibrations along the C- axis. The unpolarized Raman experiments demonstrate an oxygen weak vibrations at  $637\text{ cm}^{-1}$ , characteristic oxygen vibration for the cubic phase.

The thermal evolution and the phase behaviour has been studied by Moessbauer Spectroscopy, as well. All important Moessbauer parameters (isomer shift, quadruple splitting, line width and peak intensity) have been determined from the doublet Moessbauer spectra measured at room temperature. It was established that iron is only in Fe(III) state of octahedral  $FeO_6$  coordination. In all samples investigated the IS values of  $^{57}Fe$  are positive and close to  $0.33 \pm 0.01\text{ mm/s}$ . The  $^{57}Fe$  atoms are not spherical subordinated and possess well- expressed quadruple splitting effect. Fe(III) atoms are registered in three states: cubic (low QS values), tetragonal (middle QS values

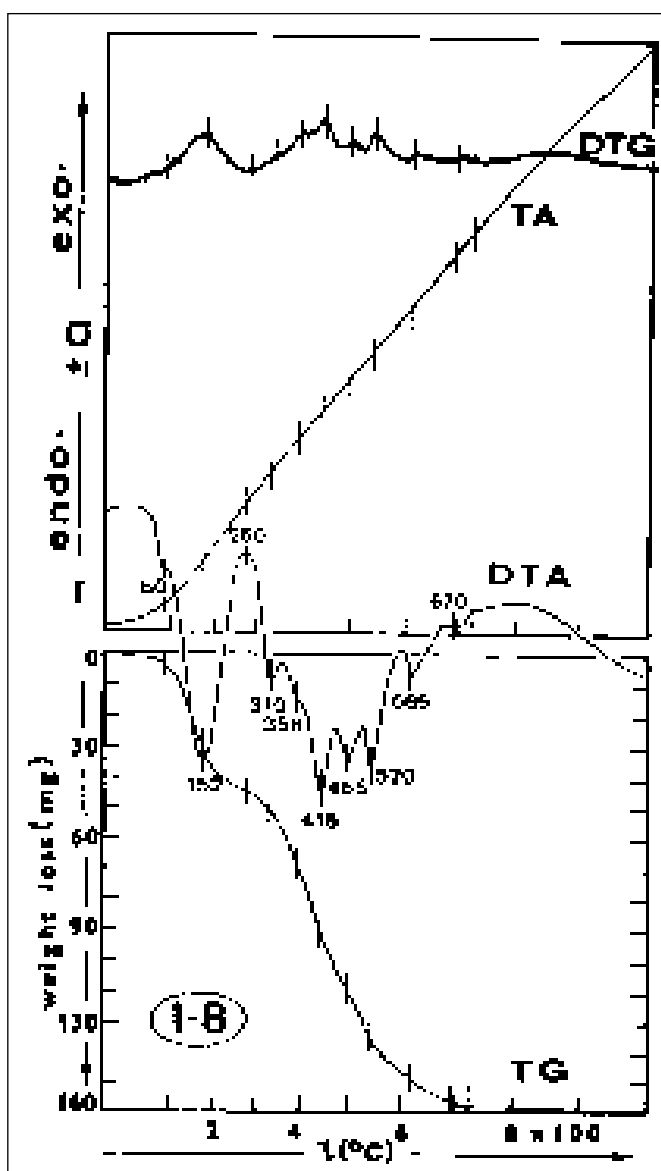


Figure 10. Thermal evolution of powder with composition  $La_{0.8}Sr_{0.2}Co_{0.8}Fe_{0.2}O_{3-\delta}$ ; DTA, TA, TG and DTG curves behaviour at heating rate of 10-C per minute.

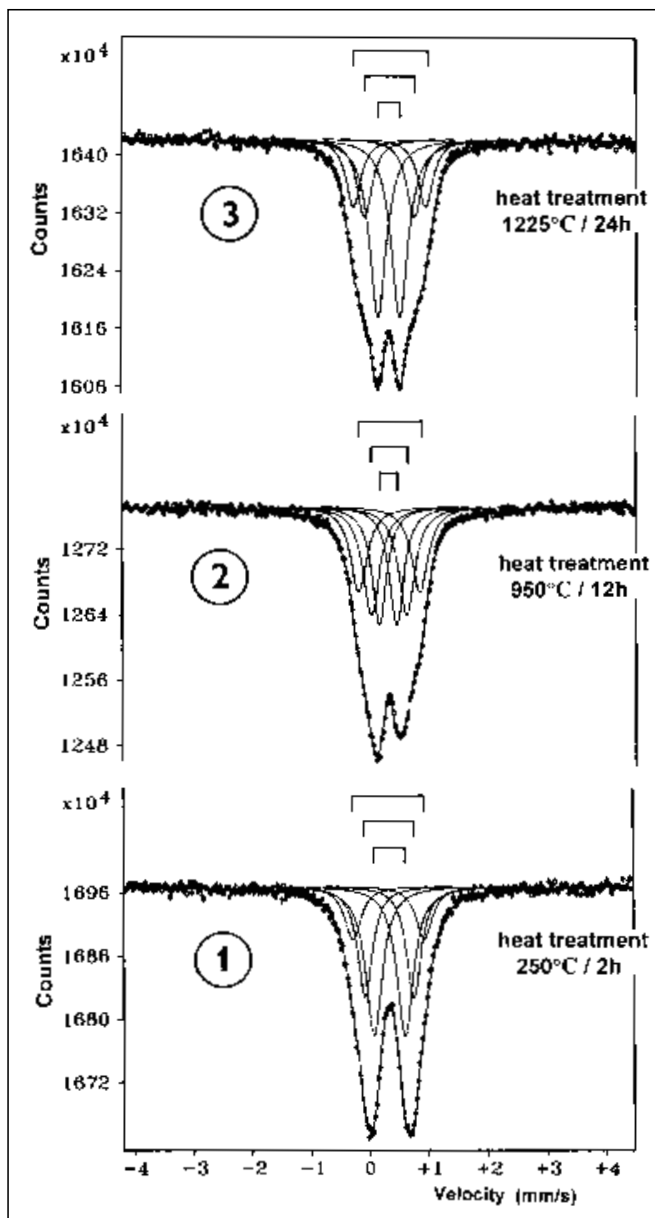


Figure 11. The  $^{57}Fe$  Moessbauer spectra at room temperature of sample I-6 -  $La_{0.6}Sr_{0.4}Co_{0.8}Fe_{0.2}O_{3-\delta}$  at different heat treatment.

and metastable highly distorted perovskite related rhombohedral- phase (high QS values). The last one is rich in oxygen vacancies. We believe that the Fe(III) atoms diffusion in the octahedral surroundings of the perovskite- like phases is almost equal ( $\bar{A}_{\text{exp}} = 0.31$ ). From structural point of view it was established that the lanthanum rich compositions and related phases are more stable at high temperature after oxygen treatment, (Figure 11).

Positron annihilation lifetime parameters indicate that the samples investigated are highly dense; not so much porous areas with 2- 3 $\mu\text{m}$  in diameters. The information is obtained from component ( $\tau_3$ ) of the longest lifetime. The values of component ( $\tau_2$ ) of the middle lifetime show limited voids of dimensions less than 2 $\bar{L}$  detected in the sample. The component of shortest lifetime ( $\tau_1$ ) is connected with both positron annihilation process and lattice vacancies' distribution, as well. It can be accepted that cation defects in the bulk exist, stimulating negative charge and effectively trap the positrons.

#### 4.5.2. SURFACE STRUCTURAL CHARACTERIZATION

Monitoring of perovskite surface is carried through ESCA-XPS (X-ray photoelectron spectroscopy). The detailed XPS survey spectra, valence band region spectra, partial core level spectra of the La, Sr, Ba, Co and Fe ions as well as O1s peak positions and behavior of the anion subnetwork are presented and discussed in [46]. The XPS experiments are carried out as function of oxygen partial pressure, thermal treatment procedure and the amount of the alkaline- earth (Sr) structural substitution. The 3d- electronic structure, surface O1s evolution and some local interactions are discussed in details.

Figure 12 shows the valence band spectra and the interactions close to the  $E_F$  level. In the valence band range there is a contribution from the metal 3d- states and BE near 6 eV arising from hybridization states of primary oxygen 2p character is registered. Close to  $E_F$  there is a mixed effect of the Co3d and Fe3d ions in the  $\text{MeO}_6^{9-}$  polyhedron (where Me= Co and Fe) related to the above 3d- derived states with BE at 2.2 eV. This effect can be explained in terms of the ionic multiplex structure of the photoionized  $3d^{n-1}$  state configuration. There was established a shifting effect from 3 eV ( $\text{LaCoO}_3$  [47]), 2.2 eV (sample  $\text{La}_{1-0.6}\text{Sr}_{0.6}\text{Co}_{0.8}\text{Fe}_{0.2}\text{O}_{3-\delta}$  figure 12) to 1.7 eV (sample  $\text{La}_{0.4}\text{Sr}_{0.6}\text{Co}_{0.8}\text{Fe}_{0.2}\text{O}_{3-\delta}$ [48]). This shift can be easily understood by noting that the Sr- substitution of the La- ions leads to doping the system with holes. The holes will populate the top levels of the occupied band, thus shifting BE to lower values. The experiments show that in the samples the Fe(III) and Co(III) a low spin state in octahedral coordination co- exists. Verify that the low spin ions are involved in the oxygen transfer process and surface oxygen exchange.

As figure 13 shows XPS scanning surface spectra which indicate the presence of all (La,Sr(Ba),Co,Fe and O) elements on the surface. All partial elements' contributions are presented and Auger lines' influence is demonstrated. The peak position and evolution vs. composition and temperature shows that the La and Co host elements are more stable on the surface than Sr(Ba) and Fe contribution[49].

The thermal and oxygen treatment influence on O1s species has been investigated, as well [46]. It was established two well resolved peaks. The first O1s ( $529.4 \pm 2\text{eV}$ ) peak is very stable and a contribution from the oxygen sublattice can be accepted. The second one at 532.4 eV is temperature sensitive. This phenomenon is due to less- electron rich species of oxygen; possi-

ble to lose the oxygen from  $\text{OH}^-$ , surface adsorbed oxygen and non- bridging oxygen from the lattice.

#### 4.6. Properties characterization

There is no attempt to discuss details about membrane properties. We like only to mention that membrane density, water-soak level, microhardness values, some electrical parameters and impedance spectroscopy study of boundary role on the conductivity reduction have been object of investigation. Grain boundary role on the electrical properties of  $\text{La}_{1-x}\text{Sr}_x\text{Co}_{0.8}\text{Fe}_{0.2}\text{O}_{3-\delta}$  perovskite samples has been investigated accurately and published in details [50]

Oxidative coupling of methane, oxygen permeation behaviour and catalytic measurements by dense inorganic membranes are perfectly reported in [12, 21].

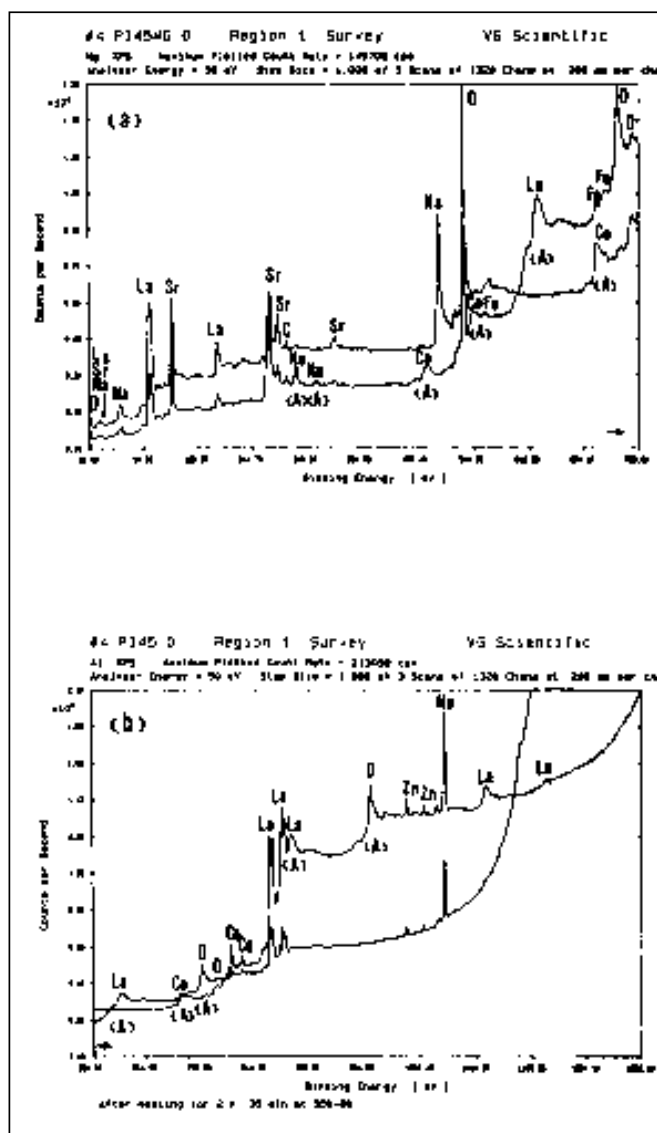


Figure 12. Valence band XPS spectrum of mixed conducting membrane with composition  $\text{La}_{0.6}\text{Sr}_{0.4}\text{Co}_{0.8}\text{Fe}_{0.2}\text{O}_{3-\delta}$ .

## 5. CONCLUSION

The review addresses up-to-date investigation of dense ceramic membranes, their possible application and modern membrane classification. The attention is focused on a new family of membranes with mixed conductivity and essential candidates for industrial application. The characteristics of the perovskite structure and oxygen ion migration via a vacancy transport mechanism is discussed. An adequate interpretation is made for surface oxygen exchange and Wagners' oxygen bulk conductivity. It was shown that the driving forces are the chemical oxygen potential ( $\Delta\mu_{O_2}$ ) which depend of the composition, temperature and  $p_{O_2}$  applied.

Some important membrane parameters and design of chemical reactors are discussed, as well.

In the author's laboratory dense ceramic membranes have been prepared by thermal evolution of powders obtained via metal nitrate solutions. It was established by phase analysis that the loss of oxygen from the lattice stimulates formation of low cell position than cubic one. Generally formation of tetragonal and rhombohedral cell. The last is temperature sensitive according to ND studies. The applied methods for structural identification serve as a useful information on macro-, micro- and superfine levels. It was established that iron is only in Fe(III) state of octahedral  $FeO_6$  coordination. In all samples investigated by Moessbauer Spectroscopy the IS values of  $^{57}Fe$  are positive and close to 0.33 mm/s. The  $^{57}Fe$  atoms are not spherical subordinated and possess well-expressed quadruple splitting effect. The XPS study shows that Fe(III) and Co(III) ions co-exists at a low spin state in octahedral coordination. Verify that the low spin ions are involved in the oxygen transfer process and surface oxygen exchange.

The review undoubtedly shows that the dense inorganic membranes are actual and nowadays rather extensively appear to be an object of study. They have become of great interest for both partial (18) and total (19) oxidation of hydrocarbons and as an effective means of producing oxygen from air [12].

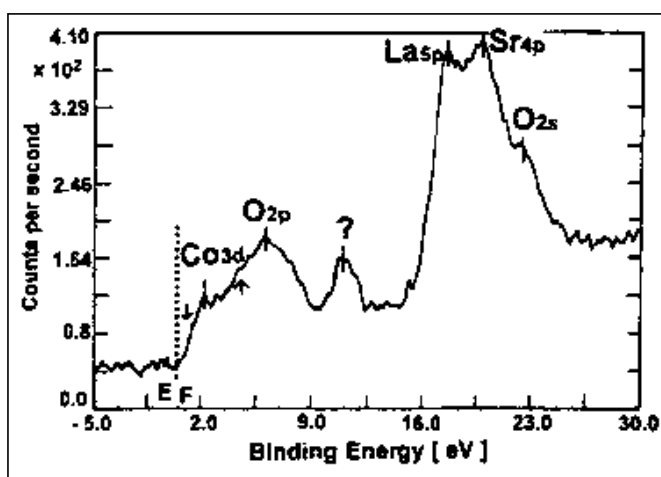


Figure 13 A correlation dependence of the survey XPS spectra obtained from  $AlK_{\alpha}$  and  $MgK_{\alpha}$  X-ray sources.

## ACKNOWLEDGMENT.

The support from the Commission of the European Communities in the frame of the JOULE II programme, is greatly acknowledged. We thank H. J. M. Bouwmeester for his activities stimulating the cooperation between University of Twente and University of Chemical Technology and Metallurgy- Sofia. J. Carda and G. Garcia- Belmonte are gratefully acknowledged for useful discussions and research carried out on dense membranes at University Jaume I, Castellon.

## REFERENCES

1. J. Charpin, A.J. Burggraaf and L. Cot. 'A survey of Ceramic Membranes for separation in liquid and gaseous media' *Industrial Ceramics* **11** [2] (1991) 84.
2. V. Kozhukharov, M. Machkova and N. Brashkova. 'CERAMIC MEMBRANES: An Update on Activity' *Proceed. 12-th Conference on Glass and Ceramics, 24-26 September 1996, Varna, Bulgaria* (1997) 370
3. K. Sing, D. Everett, R. Huel, L. Moscou, R. Rierotti, J. Rouquerol and T. Siemieniowska. 'Nomenclature for porous materials' *Pure and Appl. Chem.* **57** (1985) 603.
4. Ch. Roger, M. Hampden-Smith, D. Schaefer and G. Beaucage. 'General routes to porous metal oxides via inorganic and organic templates' *J. Sol-Gel Science & Technology* **2** (1994) 67.
5. D. Schaefer. 'Engineering porous materials' *MRS Bulletin*, April (1994) 14.
6. A. Burggraaf, H. J. Bouwmeester, B. Boukamp, R. Uhlhorn and V. Zaspalis. 'Synthesis, microstructure and properties of porous and dense ceramic membranes' *Science of Ceramic Interfaces* Ed. J. Nowotny, Elsevier Sci. Pub. B.V. (1991) 525
7. C. Vayenas, M. Jaksic, S. Bebelis and S. Neophytides. 'The electrochemical Activation of Catalytic Reactions' in *Modern Aspects of Electrochemistry*, Number **29**, Ed. by J. O'M. Bockris et al., Plenum Press, N. Y. (1996) p. 61.
8. P. Zegers. 'Status of SOFC Development in Europe' in *Proceed. of the 3-th Int. Symp. on Solid Oxide Fuel Cells*, Eds' S. Singhal and H. Iwahara, The electrochem. Soc. *Proceed.* **vol. 93-94** (1993) p.16.
9. D. Hooie. 'Status of SOFC Development in USA' in *Proceed. of the 3-th Int. Symp. on Solid Oxide Fuel Cells*, Eds' S. Singhal and H. Iwahara, The electrochem. Soc. *Proceed.* **vol. 93-94** (1993) p.3.
10. H. Tagawa. 'Status of SOFC Development in Japan' in *Proceed. of the 3-th Int. Symp. on Solid Oxide Fuel Cells*, Eds' S. Singhal and H. Iwahara, The electrochem. Soc. *Proceed.* **vol. 93-94** (1993) p.6.
11. S. P. Badwal and K. Foger. 'Status of SOFC Development in Australia' in *Proceed. of the 3-th Int. Symp. on Solid Oxide Fuel Cells*, Eds' S. Singhal and H. Iwahara, The electrochem. Soc. *Proceed.* **vol. 93-94** (1993) p. 21.
12. H. J. Bouwmeester and A. J. Burggraaf. *Fundamentals of Inorganic Membrane Science and Technology*, Membrane Science and Technology Series-4, Eds. A. Burggraaf and L. Cot, Elsevier Sci., Amsterdam- N.Y.-Tokyo (1996) 435.
13. C. Vayenas, S. Bebelis and S. Ladas. 'Dependence of catalytic rates on catalyst work function' *Nature* **343** (1990) 625.
14. S. Bebelis and C. Vayenas. 'Non-Faradaic Electrochemical Modification of Catalytic Activity: I. The case of ethylene oxidation on  $Pt^{\delta}$ ' *J. Catal.* **118** (1989) 125
15. C. Vayenas, S. Bebelis, I. Yentekakis and H. Lintz. 'NEMCA: A Status Report' *Catalysis today*; Elsevier Amsterdam **11** (1992) 303- 442.
16. Y. Teraoka, T. Nobunaga and N. Yamazoe. 'Effect of cation substitution on the oxygen semipermeability of perovskite-type oxides' *Chem. Lett.* (1988) 503
17. H. Kruidhof, H. Bouwmeester, R. van Doorn and A. Burggraaf. 'Influence of order-disorder transitions on oxygen permeability through selected nonstoichiometric perovskite-type oxides' *Solid State Ionics- Diffusion & Reactions* **63** (1993) 816.

18. T. Shimizu. 'Partial oxidation of hydrocarbons and oxygenated compounds on perovskite oxides' *Special Issue on Perovskite Oxides* Catalysis Reviews-Sci. & Eng. **34** (1992) 281- 427, Publ. by Marcel Decker, Inc., New York, Basel, Hong Kong (1992) p. 355
19. T. Seiyama. 'Total oxidation of hydrocarbons on perovskite oxides' *Properties and applications of perovskite-type oxides* Eds. L. Tejuca and J. Fierro (Marcel Decker, Inc., N.Y, Basel, Hong Kong, (1993) p.215
20. Y. Teraoka, H.-M. Zhang, S. Furukawa and N. Yamazoe. 'Oxygen permeation through perovskite-type oxides' *Chem. Lett.* (1985) 1743
21. J. E. ten Elshof. 'Dense inorganic membranes: Studies on transport properties, defect chemistry and catalytic behaviour' Ph.D. Thesis, University of Twente, Enschede, the Netherlands (1997).
22. R. H. van Doorn, E. G. Keim, T. Kachliki, H. J. Bouwmeester and A. J. Burggraaf. 'Structure modelling of  $\text{La}_{1-x}\text{Sr}_x\text{CoO}_{3-d}$  ( $x=0.5$  and  $0.7$ )' manuscript in preparation, University of Twente, Enschede, the Netherlands.
23. S. Russek. 'Air separation with Perovskite-type oxide membranes; Membrane materials consideration' Ph.D. Thesis, University of California at Berkeley, Calif., USA (1992).
24. A. Wells. 'Structurnaya neorganicheskaya khimiya' **vol.2**, Moskva, Mir (1987) p.300 (in russian)
25. 'Crystal data ; JCPDS Determinative Tables Inorganic Compounds' Eds. J. D. Donnay and H. Ondik Third Edition, **vol.2**, (1973).
26. C. Wagner. 'Beitrag zur Theorie des Anlaufvorgangs' *Z. Phys. Chem.* **21** (1933) 25- 41.
27. H. J. Bouwmeester, H. Kruidhof and A. J. Burggraaf. 'Importance of the surface exchange kinetics as rate limiting step in oxygen permeation through mixed-conducting oxides' *Solid State Ionics* **72** (1994) 185
28. L. Tejuca, J.L.Fierro and J. M. Tascon. 'Structure and reactivity of perovskite-type oxides' *Adv. Catal.* **36** (1989) 237
29. A. Searcy. *Chemical and Mechanical Behaviour of Inorganic Materials*, Eds. A. Searcy, D. Ragone and V. Colombo, Wiley- Interscience, N.Y. (1970)
30. B. A. van Hassel, T. Kawada, N. Sakai, H. Yokokawa, M. Dokiya and H. J. Bouwmeester. 'Oxygen permeation modelling of perovskites' *Solid State Ionics* **66** (1993) 295
31. V. Kozhukharov, N. Brashkova, M. Machkova and F. Dipchikov. 'Processing and development of mixed-conducting oxide membranes' *Research founded by EC JOULE Programme, Final scientific report*, May, Sofia (1996).
32. J. Frye, W. Klierer and T. Mazanec. Applicant : The standard oil company 'Electrochemical reactors and multicomponent membranes useful for oxidation reactions' *EP Patent 0 438 902*, H01M 8/12 (20-12-1990).
33. H. J. M. Bouwmeester. 'Electrochemical activation of methane using solid oxide membranes' *Fifth Periodic Joint Report to Contract No JOU2- CT92-0142*, November 1995, Enschede.
34. B. A. van Hassel, J. E. ten Elshof and H. J. Bouwmeester. 'Oxygen permeation flux through  $\text{La}_{1-y}\text{Sr}_y\text{FeO}_{3-d}$  limited by carbon monoxide oxidation rate' *Appl.Catal. A: General*, **119** (1994) 279
35. U. Balachandran, J. Dusek, S. Sweeney, R. Roepfel, R. Mieville and P. Maiya. 'Methane to syngas via ceramic membranes' *Amer. Cer. Soc. Bull.* **74** (1995) 71.
36. M. P. Harold, C. Lee, A. J. Burggraaf, K. Keizer, V. T. Zaspalis and R. S. de Lange. 'Catalysis with Inorganic Membranes' *MRS Bulletin*, April (1994) 34.
37. E. A. Hazbun. 'Ceramic membrane for Hydrocarbon Conversion' *USA num.* **4 791 079** (13-12-1988).
38. JSPDS, Mineral Powder Diffraction File' *Int. Cent. for Diffraction Data, Swarthmore USA* (1986).
39. T. Ishigaki, S. Yamanchi, J. Mizusani, K. Fueki and H. Tamura. 'Tracer diffusion coefficient of oxide ions in  $\text{LaCoO}_3$  single crystal' *J. Sol. State. Chem.* **54** (1984) 100.
40. T. Ishigaki, S. Yamanci, K. Kishio, J. Mizusani and K. Fueki. 'Diffusion of oxide ion vacancies in perovskite-type oxides' *J. Sol. State. Chem.* **73**(1988) 179.
41. H. J. Bouwmeester, H. Kruidhof and A. J. Burggraaf. 'Importance of the surface exchange kinetics as rate limiting step in oxygen permeation through mixed-conducting oxides' *Proceed. Solid State Ionic Symp.*, 12-17 Sept., The Hague, The Netherlands. (1993) 32
42. J. Kirchnerova and D. Hibbert. 'Structure and properties of  $\text{La}_{1-x}\text{Sr}_x\text{CoO}_{3-g}$  prepared by freeze drying' *J. Mat. Sci.* **28** (1993) 5800.
43. S. Neov, R. Sonntag, V. Kozhukharov, D. Neov, H. Bouwmeester. 'Neutron diffraction investigation of perovskite membranes' *Proceed. Experimental Report* (1996) p.143
44. S. Neov, R. Sonntag, V. Kozhukharov and J. E. ten Elshof. 'Crystal and magnetic structure of substituted lanthanum cobaltites' *Proceed. BENSOC Experimental Report* (1997) p. 31
45. R. Sonntag, S. Neov, V. Kozhukharov, D. Neov and J. E. ten Elshof. 'Crystal and magnetic structure of substituted lanthanum cobaltites' *Physica B* **241-243** (1998) 393
46. M. Machkova, N. Brashkova, P. Ivanov, J. B. Carda and V.Kozhukharov. 'Surface behaviour of Sr-doped lanthanide perovskites' *Appl. Surface Science*, **119** ( 1997) 127.
47. D. Sarna and A. Chainani. 'Electronic Structure of perovskite oxides,  $\text{LaMO}_3$  ( $M= \text{Ti} - \text{Ni}$ ), from High Energy Electron Spectroscopic investigations' *J. Sol. State Chem.* **111** (1994) 208.
48. V. Kozhukharov, N. Brashkova, M. Machkova and F. Dipchikov. 'Processing and development of mixed-conducting oxide membranes' *Second scientific report*, Sofia, April(1995) p. 16.
49. V.Kozhukharov, M. Machkova, P. Ivanov, H. Bouwmeester and R. van Doorn. 'Surface analysis of doped lanthanide cobalt perovskites by X-ray Photoelectron Spectroscopy' *J. Mater. Sci. Lett.* **15** (1996) 1727.
50. G. Garcia-Belmonte, F. Fabregat, J. Bisquert, V.Kozhukharov and J.Carda 'Grain boundary role in the electrical properties of  $\text{La}_{1-x}\text{Sr}_x\text{Co}_{0.8}\text{Fe}_{0.2}\text{O}_{3-\delta}$  perovskites' *Solid State Ionics*, **107** (1998) 203

Recibido: 22-7-97

Aceptado: 16-8-98

